2013 IEEE/RSJ International Conference on
Intelligent Robots and Systems (IROS)
November 3-7, 2013. Tokyo, Japan

Model discrepancy in robotic calibration: its influence on the experimental parameter identification of a parallel space telescope

Thibault Gayral[1], David Daney[+,1], Marc Bernot[2]

Abstract— **The model of a robot may not be able to consider all the physical phenomena influencing the manipulator performances since they are too numerous and/or difficult to measure: this is model discrepancy. For a highly-accurate active space telescope, an important source of inaccuracy was measured using photogrammetry: the deformation of its mobile platform. This deformation cannot be directly measured in space and needs to be properly modeled in order to enable the telescope calibration with the available measurements. Two incremental models are proposed and the parameter observability is discussed. After experimental calibration, a micrometer accuracy can be reached. The influence of model discrepancy on the experimental parameter identification is finally discussed.**

Index Terms— **Calibration; Model discrepancy; Parallel robot; Flexure joints; Micrometer accuracy; Observability**

I. Introduction

Robotic calibration aims at improving the robot accuracy through identification of its model parameters. However, the robot model can only approximate the real robot behavior. Indeed, many sources of inaccuracy influence the inner working of the robot. The inaccuracy sources classically considered are geometric, static, dynamic and non-geometric errors due to environmental interactions.

Identifying all the sources of inaccuracy, even if possible, will require the use of a huge number of specific sensors that are themselves inaccurate (e.g. static calibration is often performed using force or frequency sensors [1], [2]). Because of the cost and difficulty of such a procedure, many studies were performed to analyze the main sources of inaccuracy that need to be considered in the robot modeling [3]–[5]. However, these analyses conclude that influence of systematic errors on the robot accuracy mostly depend on the robot application, manufacturing tolerances and environmental conditions, which means that no *a priori* can be given on the influence of one or another inaccuracy source.

Moreover, such models deal with the main sources of inaccuracy only. So model discrepancy will exist in almost all robotic calibration. Since calibration compares measurements and results issued from a model prediction, those errors are accounted in the model parameter identification [6]. A possible consequence is an identified parameter value drastically different from its nominal one and even unrealistic, while providing good accuracy results. The experimental calibration of an active space telescope highlights this phenomenon, and the influence of model discrepancy on calibration results can be explained in this case.

[+]Corresponding author: david.daney@inria.fr
[1]INRIA Sophia Antipolis, France
[2]Thales Alenia Space Cannes, France

II. Model Discrepancy in Calibration

Without loss of generality, we will only focus on kinematic calibration. Let consider a manipulator, with either a closed or open kinematic chain, with n' actuators controlling n degrees of freedom ($n \leq n'$). The exact pose p of the end-effector is described by the n-vector $\mathbf{x}_p^*$, and ρ_p^* stands for the n'-vector of the exact joint coordinates at pose p. The exact kinematic model of this robot relates the joint and end-effector coordinates ρ_p^* and $\mathbf{x}_p^*$ through a function $\mathbf{f}^*$ that depends upon the m_{tot} exact model parameters described by the vector ξ_{tot}^*:

$$\mathbf{f}^*(\mathbf{x}_p^*, \rho_p^*, \xi_{\text{tot}}^*) = \mathbf{0} \tag{1}$$

The exact kinematic model takes into account all the sources of inaccuracy that influence the robot kinematic behavior (e.g. stiffness, temperature, humidity, etc). However, such a model may be too complex, or even too difficult to obtain. Thus, the kinematic model is often simplified through a function $\mathbf{f}$ depending upon m exact parameters, with $m < m_{\text{tot}}$, described by the vector ξ^*. In this case, the inaccuracy sources not considered in $\mathbf{f}$ can be taken into account in an additive discrepancy function ε_f [7]:

$$\mathbf{f}(\mathbf{x}_p^*, \rho_p^*, \xi^*) = \varepsilon_f(\mathbf{x}_p^*, \xi^*, \xi_{\text{tot}}^*) \quad \text{, with } \varepsilon_f = \mathbf{f} - \mathbf{f}^* \tag{2}$$

It may be assumed that the kinematic parameters ξ are known with uncertainties $\delta\xi^*$ due to manufacturing and assembly errors, such as $\xi = \xi^* + \delta\xi^*$. The purpose of kinematic calibration is to improve the robot accuracy through identification of its model parameters. In a calibration process, measurements $\mathbf{y}_p^*$ on the robot state are obtained for different poses $\mathbf{x}_p^*$, with $p = 1..N_p$. Those measurements are related to the model parameters ξ^* through an identification function $\mathbf{g}_p$ of pose p, issued from the kinematic model $\mathbf{f}$:

$$\mathbf{g}_p(\mathbf{y}_p^*, \rho_p^*, \xi^*) = \varepsilon_g^p \quad \text{, with } \varepsilon_g^p = \varepsilon_g(\mathbf{x}_p^*, \xi^*, \xi_{\text{tot}}^*) \tag{3}$$

where ε_g^p considers the model discrepancy of pose p.

Considering a sufficient number of measurements $\mathbf{y}_p^*$, the kinematic parameters ξ can be estimated by minimizing a function of $\mathbf{g}_p$ over all the calibration poses p. A common way to perform calibration is to use non-linear least square algorithm [8] in order to minimize $\sum_{p=1}^{N_p} \mathbf{g}_p^T \mathbf{g}_p$. However, measurements also contain errors $\delta\rho_p^*$ and $\delta\mathbf{y}_p^*$ such as $\rho_p = \rho_p^* + \delta\rho_p^*$ and $\mathbf{y}_p = \mathbf{y}_p^* + \delta\mathbf{y}_p^*$. Accordingly, a linear approximation of $\mathbf{g}_p$ for the least square algorithm is:

$$\mathbf{g}_p(\mathbf{y}_p, \rho_p, \xi) = \varepsilon_g^p + \mathbf{G}_y^p \delta\mathbf{y}_p^* + \mathbf{G}_\rho^p \delta\rho_p^* + \mathbf{G}_\xi^p \delta\xi^* \tag{4}$$

where Jacobian matrices $\mathbf{G}_x^p = \partial\mathbf{g}_p/\partial\mathbf{x}$ depend on the pose p. Nonetheless, the exact values of $\delta\mathbf{y}_p^*$ and $\delta\rho_p^*$ are not

known and cannot be identified since identifying either $\delta \mathbf{y}_p^*$ or $\delta \rho_p^*$ prevent the identification of $\delta \xi^*$ due to their number. Thus, the identification process is always performed under the hypothesis that $\mathbf{g}_p$ mostly depends on the variation $\delta \xi^*$ of the model parameters. This yields to, with $\delta \xi \neq \delta \xi^*$ since $\delta \xi$ considers the measurement noise and sensor inaccuracy:

$$\mathbf{g}_p(\mathbf{y}_p, \rho_p, \xi) \approx \varepsilon_g^p + \mathbf{G}_\xi^p \delta \xi \tag{5}$$

Hence, minimizing $\sum_{p=1}^{N_p} \mathbf{g}_p^T \mathbf{g}_p$ will implicitly lead to values of $\delta \xi$ accounting for the model discrepancy ε_g. In case of an important model discrepancy, this may yield to parameter values being far away from their nominal ones. Those issues are highlighted and explained in the experimental accurate calibration of an active space telescope described below.

III. Description of the Space Telescope

Based on a parallel architecture, the telescope structure makes possible the repositioning of the secondary mirror (M2) relatively to the primary one (M1) in space. Due to its active structure, the optical quality of the telescope can be optimized contrary to traditional space telescopes. To achieve this accurate positioning, a proper model of the telescope is required, ensuing a need for calibration.

A. Kinematic structure

The device is a 6-PUS parallel robot shown in Fig. 1 and patented by INRIA [9], with all prismatic actuators linked to the base and in a vertical position, where P, U and S stands for prismatic, universal and spherical joints, respectively.

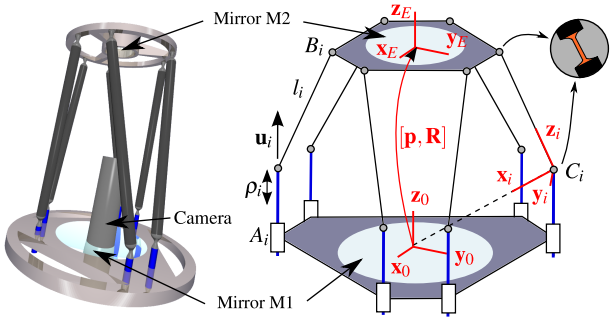

Fig. 1: Active wrist platform and definition of notations

Frames $\mathscr{F}_o = (\mathbf{x}_o, \mathbf{y}_o, \mathbf{z}_o)$ and $\mathscr{F}_E = (\mathbf{x}_E, \mathbf{y}_E, \mathbf{z}_E)$ are attached to the base and the mobile platform, respectively. Those frames are linked together through a position vector $\mathbf{p}$ and a rotation matrix $\mathbf{R}$ which describe the position and orientation of $\mathscr{F}_E$ with respect to $\mathscr{F}_o$.

The base and mobile platforms are linked together through 6 legs of fixed length $l_i \approx 0.5$ m, with $i = 1...6$. Each leg i is attached at one side to the mobile platform at point $\mathbf{b}_i$, whose coordinates are given in the mobile frame $\mathscr{F}_E$, and to point $\mathbf{c}_i$ at the other side. Coordinates of point $\mathbf{c}_i$ are always given in the base frame $\mathscr{F}_o$ and follow the relation $\mathbf{c}_i = \mathbf{a}_i + \rho_i \mathbf{u}_i$ where ρ_i relates the displacement of actuator i along direction $\mathbf{u}_i$ and $\mathbf{a}_i$ stands for the attachment point of the i^{th} actuator on the base platform. To each leg i a frame $\mathscr{F}_i = (\mathbf{x}_i, \mathbf{y}_i, \mathbf{z}_i)$ is attached, where $\mathbf{z}_i$ is the principal direction of the leg and $\mathbf{x}_i$ is such as $\mathbf{z}_o$ belongs to the plane $(\mathbf{c}_i, \mathbf{x}_i, \mathbf{z}_i)$.

The design geometry is given in Fig. 2, with design parameters α_0, r_0, α_E and r_E.

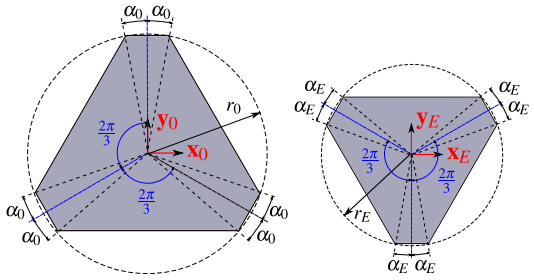

Fig. 2: Geometry of the base and the mobile platforms

B. 6-PUS model

For the telescope to be compatible with the aerospace environment, circular-arc-fillet hinge flexible joints [10] are considered in place of U and S joints, as shown in Fig. 1. Previous work showed that those flexure joints can be modeled by pure spherical joints due to the small workspace of the telescope [11]. Thus, considering each body part to behave as rigid bodies, the telescope can be modeled as a perfect 6-PUS parallel robot. Considering the leg orientations $\mathbf{z}_i$, the kinematic model $\mathbf{f}_i$ of leg i can be derived from the geometrically closed-loop equations:

$$\mathbf{f}_i = \mathbf{p} + \mathbf{R}\mathbf{b}_i - \mathbf{a}_i - \rho_i \mathbf{u}_i - l_i \mathbf{z}_i \tag{6}$$

The set of model parameters $\xi = [\mathbf{a}_i^T, \mathbf{b}_i^T, \mathbf{u}_i^T, l_i]^T$ for each leg i is sufficient to completely describe the model.

C. Specifications

The space telescope does not manipulate any payload and only needs a small workspace. The device workspace W and desired accuracy are given in table I. Workspace requirements of the device do not consider θ_z since motions around $\mathbf{z}_E$ do not influence the image quality provided by the telescope due to the mirror sphericity.

	x (mm)	y (mm)	z (mm)	θ_x (°)	θ_y (°)
Workspace	2	2	0.2	1	1
Desired Accuracy	0.1	0.1	0.01	0.05	0.05

TABLE I: Requirements of the telescope

For the device to fit the requirements, the motor ranges are set to $\Delta\rho_i = \pm 1.3$ mm with an accuracy of ± 1 μm. Considering a perfect 6-PUS with dimensions of Fig. 2, a pose accuracy of, at worst, 6 μm and 10^{-6} degree was calculated over the entire workspace.

However, a model discrepancy from the perfect 6-PUS model was experimentally identified: the mobile platform deformation. Moreover, the model parameters are not known exactly: for the accurate calibration, a proper choice of the measurement configurations is needed. Finally, the effect of model discrepancy on calibration results are discussed.

IV. Model Discrepancy: The Mobile Platform Deformation

For calibration, measurements were performed on the entire telescope structure through photogrammetry: the position of each object point attached to the telescope was obtained in the measurement frame, as shown in Fig. 3. A first analysis of the photogrammetry object point displacements shows a deformation of the mobile platform of the telescope. A linear and a matrix approximation are developed below to highlight the impact of model discrepancy on the identification of the model parameters. Note that more complex models such as a stiffness model were also studied but no final accuracy improvement was obtained due to observability issues.

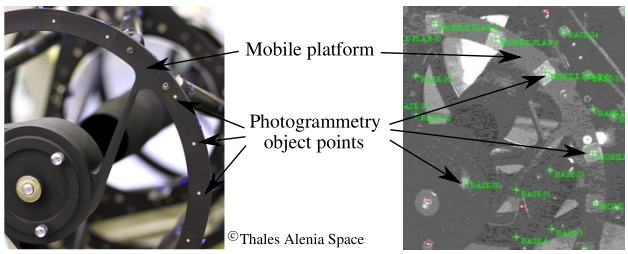

Fig. 3: Experimental setup of photogrammetry

The algorithm proposed by Haralick *et al.* is considered [12] in order to extract the position and the orientation of each rigid body of the telescope structure from photogrammetry object points. This method gives the rigid displacements of a scatter of points between two poses with noise considerations. The data analysis validates the rigid body hypothesis on all bodies, except for the mobile platform – deformations up to 60 μm from a rigid model were observed.

Fig. 4 illustrates a deformation of the ring on which the legs are attached at points $\mathbf{b}_i$. The deformed ring looks like a buckled wheel for almost all measurement configurations. Such a deformation is due to the flexible joints that generate stresses. The measured deformations at points $\mathbf{b}_i$ are higher than the 5 μm given by simulations and lead to an unacceptable inaccuracy.

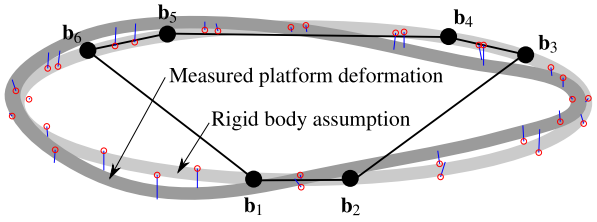

Fig. 4: Measured deformation of the mobile platform for one measurement configuration. Blue lines represent the amplified error between the measured object points and their rigid body position estimation (red circle points).

A. Linear approximation of the model discrepancy

A linear model is first proposed in order to evaluate the displacements Δb_i^z of points $\mathbf{b}_i$. Fig. 5 shows the measured displacements Δb_i^z of points $\mathbf{b}_i$ in the measurement frame plotted as functions of the actuator displacements $\Delta\rho_i$. Due to the small displacements Δb_i^z (± 60 μm), a linear relation between Δb_i^z and $\Delta\rho_i$ is assumed, considering the coefficient κ_i with initial value identified at 0.011 for $i = 1...6$:

$$\Delta b_i^z = \kappa_i \Delta\rho_i \tag{7}$$

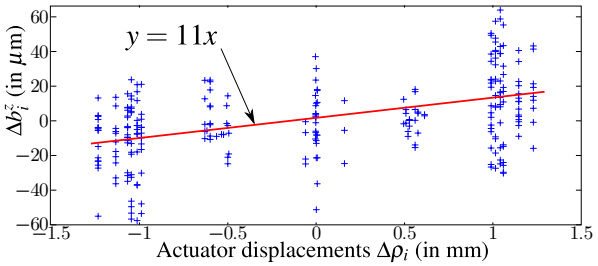

Fig. 5: Linear approximation of the platform deformation

B. Matrix approximation of the model discrepancy

The mobile platform deformation is due to the stresses generated by the flexure joints. Those stresses depend on the static equilibrium of the mobile platform which involves all forces acting on the platform at points $\mathbf{b}_i$. Moreover, those forces should mostly depend on the actuator displacements $\Delta\rho_i$ inducing deformations of the flexure joints. So, displacements of point $\mathbf{b}_i$ must be related to the actuator displacements through a coefficient matrix $\mathbf{K}$:

$$\Delta\mathbf{b}^z = \mathbf{K}\Delta\rho \tag{8}$$

with $\Delta\mathbf{b}^z = [\Delta b_1^z ... \Delta b_6^z]^T$, and $\Delta\rho = [\Delta\rho_1 ... \Delta\rho_6]^T$. In order to identify the terms of the coefficient matrix $\mathbf{K}$, data from Fig. 5 is considered and distances between the measured displacements Δb_i^z and the matrix estimate are minimized through a least-square optimization. For each leg i, the i^{th} row $\mathbf{k}_i$ of matrix $\mathbf{K}$ is used to compute the displacements Δb_i^z with (9). This gives an initial estimate of the coefficient matrix $\mathbf{K}$:

$$\Delta b_i^z = \mathbf{k}_i \Delta\rho \tag{9}$$

$$\mathbf{K} = 10^{-3}\begin{bmatrix} 16 & 0 & -8 & 12 & -2 & -20 \\ 0 & 20 & -17 & -1 & 13 & -13 \\ -2 & -15 & 14 & 2 & -9 & 9 \\ 6 & -12 & 4 & 14 & -16 & 2 \\ -12 & 7 & 0 & -15 & 14 & 4 \\ -20 & -1 & 10 & -10 & 2 & 19 \end{bmatrix} \tag{10}$$

The elements of $\mathbf{K}$ are of the same order of magnitude as κ_i. Analyzing matrix $\mathbf{K}$, strong dependencies between legs 1-6, 2-3, and 4-5 are observed. For example, displacements $\Delta\rho_1$ and $\Delta\rho_6$ greatly influence Δb_1^z and Δb_6^z. This may be due to the mobile platform geometry. Indeed, there is no strengthening for the mobile platform ring between the attachment points of legs 1 and 6. Thus, displacements of point $\mathbf{b}_1$ can have a significant impact on Δb_6^z.

With the matrix model, the maximal error committed on the displacement estimation of Δb_i^z is 20 μm, and the average error is 5 μm, which is close to the measurement noise.

V. Measurement Configuration Choice

For calibration, photogrammetry was chosen as a measurement system because of its high accuracy (3 μm of standard deviation) over a wide number of object points. In order to minimize the influence of non-geometric parameters not considered in the device models [13], the photogrammetry process is performed in a clean room under controlled pressure, temperature and humidity conditions. However, the desired accuracy of 10 μm is only three times the standard deviation of the photogrammetry process. Thus, the sensitivity of calibration to measurement noise has to be as low as possible. One way to perform this task is through a proper choice of the measurement configurations [14]. Algorithms of configuration choice are always based on observability indices [15], [16] which are based on properties of the observability matrices $\mathbf{G}_\xi^p$ [17], for $p = 1..N_p$.

In order to develop the observability matrix $\mathbf{G}_\xi^p$, the 6-PUS model is considered. The identification function $g_{i,p}$ for the i^{th} leg in the p^{th} measurement configuration is derived from the closed-loop equation (6):

$$g_{i,p} = l_i - \|\mathbf{p}^p + \mathbf{R}^p\mathbf{b}_i - \mathbf{a}_i - \rho_i^p\mathbf{u}_i\| \tag{11}$$

Analyses [11] show that due to the measurement noise and the small orientation workspace of the telescope, the three model parameters $\{a_i^z, b_i^z, l_i\}$ are linearly related in the equations of calibration. Thus, among those three parameters, only one can be identified. Considering the assembly and manufacturing tolerances, it was found that l_i supports the maximal uncertainties among those three parameters. Therefore, we choose to identify l_i. Note that $\mathbf{u}_i$ is a unit vector and thus can be fully described by only two of its components u_i^x and u_i^y. The set of identifiable parameters is thus reduced to $\{a_i^x, a_i^y, b_i^x, b_i^y, u_i^x, u_i^y, l_i\}$ for each leg i. Differentiating $g_{i,p}$ with respect to the 7 identifiable parameters gives the i^{th} row of the observability matrix $\mathbf{G}_\xi^p$ of pose p:

$$(\mathbf{G}_\xi^p)_i = \left[\frac{\mathbf{h}_{i,p}^T}{2\sqrt{\mathbf{h}_{i,p}^T\mathbf{h}_{i,p}}}\begin{bmatrix}1 & 0 & & & \rho_i^p & 0\\ 0 & 1 & -\mathbf{x}_E^p & -\mathbf{y}_E^p & 0 & \rho_i^p\\ 0 & 0 & & & 0 & 0\end{bmatrix}, 1\right] \tag{12}$$

with $\mathbf{h}_{i,p} = \mathbf{p}^p + \mathbf{R}^p\mathbf{b}_i - \mathbf{a}_i - \rho_i^p\mathbf{u}_i$.

In order to determine the N_p optimal measurement configurations, we choose to consider the observability index O_1, the determinant of $\mathbf{G}_\xi^T\mathbf{G}_\xi$ with $\mathbf{G}_\xi = [\mathbf{G}_\xi^{1\,T} \dots \mathbf{G}_\xi^{N_p\,T}]^T$ since it considers all the singular values of $\mathbf{G}_\xi^T\mathbf{G}_\xi$ allowing to obtain an optimum within reasonable computation time [16]. Considering measurements of the position and orientation of the mobile platform, at least 8 measurement configurations are needed for calibration of the 6-PUS model. However, in order to improve the telescope accuracy, some other inaccuracy sources might have to be considered – for example the platform deformation as shown in this paper. Consequently and for safety reasons, calibration was performed on $N_p = 40$ measurement configurations. The optimal configurations were found to be at or very close to the boundaries of the telescope workspace. They are given in [11].

VI. Parameter Identification

The last step of a calibration process is parameter identification. From the kinematic model and the measurements, the model parameters are estimated so that an identification function $\mathbf{g}_p$ is minimized on all the measurement configurations p, with $p = 1..N_p$. In parallel robotics, identification functions are often issued from the geometrically closed-loop equations and thus are distance equations. A common way to achieve identification is the use of non-linear least square algorithms. Moreover, for the telescope under consideration, each leg can be considered separately in the equations. Thus, for the i^{th} leg, the least square equation to be minimized becomes:

$$G_i = \sum_{p=1}^{N_P} \mathbf{g}_{i,p}^T\mathbf{g}_{i,p} \tag{13}$$

with $\mathbf{g}_{i,p}$ the identification function for the i^{th} leg in the p^{th} measurement configuration.

Experimental calibration is performed with measurements of the position and orientation of the mobile platform provided from photogrammetry data, which will be the only measurements available in space. The mobile platform is considered as a perfect rigid body, and with the linear and matrix approximations, respectively. Identification uses the *lsqnonlin* function of MATLAB. Same results are obtained by using either the Levenberg-Marquardt or the trust-region reflective algorithms. Experiments show that, in our case, those algorithms are not sensitive to changes on the initial values. The observability issues are considered below.

A. With the rigid body assumption

The 6-PUS model is assumed by regarding each part of the telescope to behave as a rigid body and the identification function $g_{i,p}$ is (11). Experimental calibration confirms that only one parameter among $\{a_i^z, b_i^z, l_i\}$ can be identified. Regarding the actuator orientation $\mathbf{u}_i$, only one of its components can be experimentally identified due to observability issues, whatever parametrization used. Since identifying either u_i^x or u_i^y does not change the experimental calibration results, we arbitrarily choose to identify u_i^x. The set of identifiable parameters is thus reduced to $\{a_i^x, a_i^y, b_i^x, b_i^y, u_i^x, l_i\}$, and a_i^z, b_i^z and u_i^y are fixed to their nominal values: zero.

B. With the linear approximation of the model discrepancy

In order to take into account the linear approximation in the robot model, the identification function becomes:

$$g_{i,p} = l_i - \|\mathbf{p}^p + \mathbf{R}^p(\mathbf{b}_i + \kappa_i\Delta\rho_i^p\mathbf{z}_o) - \mathbf{a}_i - \rho_i^p\mathbf{u}_i\| \tag{14}$$

As for the 6-PUS model, a strong dependency between a_i^z, b_i^z and l_i is observed. Experiments also show that the actuator direction u_i^x and the coefficient κ_i cannot be both identified. Identifying either u_i^x or κ_i leads to the same accuracy results. Thus, we choose to identify κ_i while setting u_i^x to zero since it is directly related to the platform deformation that needs to be estimated. The set of identifiable parameters is then $\{a_i^x, a_i^y, b_i^x, b_i^y, l_i, \kappa_i\}$, and a_i^z, b_i^z, u_i^x and u_i^y are fixed to zero.

C. With the matrix approximation of the model discrepancy

Considering the i^{th} row $\mathbf{k}_i$ of the coefficient matrix $\mathbf{K}$, the identification function $g_{i,p}$ for each leg i becomes:

$$g_{i,p} = l_i - \|\mathbf{p}^p + \mathbf{R}^p(\mathbf{b}_i + (\mathbf{k}_i \Delta\rho^p)\mathbf{z}_o) - \mathbf{a}_i - \rho_i^p \mathbf{u}_i\| \quad (15)$$

As for the linear approximation, $\mathbf{k}_i$ and u_i^x cannot be both identified. Moreover, setting u_i^x to its nominal value allows the identification of only one coefficient in $\mathbf{k}_i$. Experiments show that the best accuracy results are obtained by identifying all the diagonal terms of $\mathbf{K}$, which actually relate to the coefficients κ_i of the linear model. The diagonal terms of matrix $\mathbf{K}$ are identified and are referred as κ_i in table II.

VII. Experimental Results

Table II presents the experimental results of identification for the three considered models as distances between the nominal and identified values of each identifiable parameter.

i	1	2	3	4	5	6
Δa_i^x	0.98	−0.23	−2.72	−2.31	0.37	4.42
Δa_i^y	2.62	2.57	−2.55	−1.97	−1.76	−2.42
Δb_i^x	3.59	0.73	−0.09	2.45	−3.67	−0.49
Δb_i^y	−1.38	−0.88	4.22	1.39	−0.02	3.04
Δu_i^x	−0.07	0.05	0.10	−0.06	0.05	−0.15
Δl_i	0.95	0.07	1.53	0.50	0.63	1.22

(a) Without considering the platform deformation

i	1	2	3	4	5	6
Δa_i^x	0.32	0.29	−1.74	−2.93	0.89	2.95
Δa_i^y	2.66	2.60	−2.54	−1.99	−1.71	−2.40
Δb_i^x	3.59	0.72	−0.09	2.43	−3.72	−0.44
Δb_i^y	−1.34	−0.87	4.24	1.40	0.01	3.02
Δl_i	0.91	0.05	1.48	0.48	0.62	1.11
$10^3 \Delta\kappa_i$	7.10	1.60	−0.61	1.62	−0.72	6.48

(b) With the linear approximation

i	1	2	3	4	5	6
Δa_i^x	−1.71	0.41	0.30	−1.58	−0.18	−0.34
Δa_i^y	−0.33	−0.21	−2.12	0.37	0.98	−2.62
Δb_i^x	0.56	1.91	0.04	0.41	−1.82	−0.32
Δb_i^y	−0.19	−0.21	2.25	1.46	0.61	−0.22
Δl_i	0.37	−0.45	1.02	0.25	0.43	0.58
$10^3 \Delta\kappa_i$	9.58	1.96	4.44	3.33	0.67	6.99

(c) With the matrix approximation

TABLE II: Distances between nominal and identified parameter values for the three considered models (in mm except for $\Delta\kappa_i$ which is dimensionless)

Experimental results are also given in term of final accuracy for each identified model in Fig. 6. The nominal model stands for the 6-PUS model with the initial values of the parameters. The position error refers to the distance between the calculated and the measured position of the center of the mobile platform. The orientation error is the angle of the axis-angle representation between the calculated and the measured orientation of the mobile frame $\mathscr{F}_E$. For verification purpose, 6 verification poses were chosen arbitrarily within the telescope workspace. Each bar has the size of the maximal error and the inner line stands for the average error. For the verification poses, the average and maximal error values are provided.

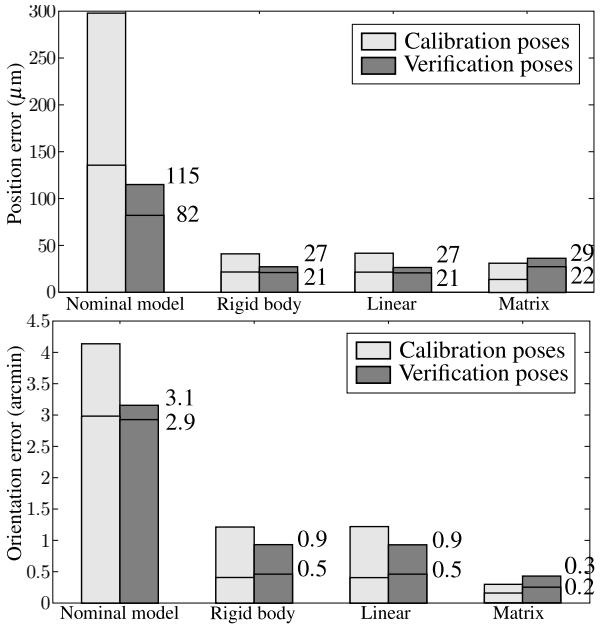

Fig. 6: Position and orientation errors, values correspond to the average and maximal errors on the verification poses

Fig. 6 shows that the desired accuracy can be reached with all models, after calibration. A better orientation accuracy is however obtained with the matrix model. Fig. 6 also shows that identical accuracy results are obtained for the rigid body assumption and the linear approximation. Moreover, the identified values for those two models are quite similar, as shown in table II. However, the identified values of u_i^x for the rigid body model are far away from their nominal values. Actually, the model discrepancy was directly taken into account in a linear approximation during the identification of the rigid body parameters in order to best fit the measurements. This can be analytically explained considering the identification function of the linear model:

$$g_{i,p} = l_i - \|\mathbf{p}^p + \mathbf{R}^p(\mathbf{b}_i + \kappa_i \Delta\rho_i^p \mathbf{z}_o) - \mathbf{a}_i - \rho_i^p \mathbf{u}_i\| \quad (16)$$

Because of the small workspace of the telescope, the platform orientation does not vary too much. Thus, the approximation of $\mathbf{R}^p(\kappa_i \Delta\rho_i^p \mathbf{z}_o)$ by $(\kappa_i \Delta\rho_i^p \mathbf{z}_o)$ leads to maximal errors of less than 1 μm for $p = 1...N_p$. Moreover, since $\mathbf{u}_i$ was set to its nominal value $\mathbf{z}_o$, (16) can be rewritten as:

$$g_{i,p} = l_i - \|\mathbf{p}^p + \mathbf{R}^p \mathbf{b}_i - \mathbf{a}_i - (\rho_i^p - \kappa_i \Delta\rho_i^p)\mathbf{u}_i\| \quad (17)$$

Considering $\rho_i^p = \rho_i^0 + \Delta\rho_i^p$ leads to:

$$g_{i,p} = l_i - \|\mathbf{p}^p + \mathbf{R}^p \mathbf{b}_i - \mathbf{a}_i - \rho_i^0 \mathbf{u}_i - (1-\kappa_i)\Delta\rho_i^p \mathbf{u}_i\| \quad (18)$$

The term $(1-\kappa_i)\Delta\rho_i^n \mathbf{u}_i$ shows that when the mobile platform deformation is not considered, the identification of κ_i is accounted in the identification of $\mathbf{u}_i$. This ensues values of u_i^x being far away from their nominal values as shown in table II. It also explains why only one component of $\mathbf{u}_i$ can be identified in the perfect 6-PUS model. Indeed, the identification process considers the platform deformation in a linear approximation for the identification of the actuator

direction $\mathbf{u}_i$. Since the linear approximation is only one degree of freedom, only one component of $\mathbf{u}_i$ can be identified.

However, the mobile platform deformation is also accounted in the other identified parameters as shown on Fig. 7. Errors between the nominal values and the identified parameters are amplified in Fig. 7 to highlight those deviations.

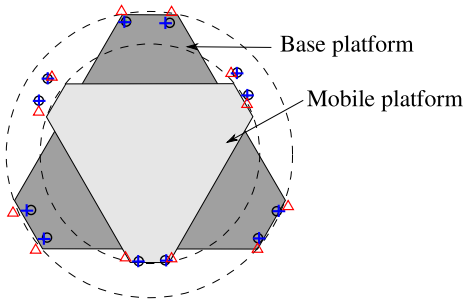

Fig. 7: Representation of errors between nominal and identified parameters values for the three different models: with the rigid body assumption (circle), the linear (cross) and the matrix model (triangle)

Fig. 7 shows that the minimum deviations from the nominal parameters are obtained as the matrix model is considered for the mobile platform deformation (points marked by triangles). This result is as expected since the matrix model is a good approximation of the mobile platform deformations. Thus, this inaccuracy source does not need to be accounted in the parameter identification and their identified values can be close to their nominal ones.

For the rigid body and linear models, we remark that the identified positions of points $\mathbf{a}_i$ and $\mathbf{b}_i$ do not correspond to the initial design of the telescope. For example, the identified geometry of the base platform considers a smaller design parameter α_0 than its initial design. Once again, the origin of those modifications must be the platform deformation: errors that cannot be taken into account in the identification of $\mathbf{u}_i$ are accounted in the other identified parameters.

VIII. Conclusions

Two models were developed to take into account the mobile platform deformation of the highly-accurate space telescope: a linear and a matrix approximation. With the matrix approximation, small deviations of the identified parameter values from their *a priori* are observed, which means that this model properly handles the mobile platform deformation. Using the linear model and without considering the mobile platform deformation, the identified parameter values are found to be "far away" from their nominal values. Those deviations are not only due to geometric uncertainties on the telescope parameters but mainly due to the model discrepancy accounted in the parameter identification. The way calibration carries the model errors over the identified parameters is analytically explained.

Experiments also show that the desired accuracy is reached with all models, on both the calibration and verification poses, which means that good accuracy results can be obtained when model discrepancy exists. However, when dealing with model parameters far away from their nominal values, (i) it is difficult to certify the device accuracy over its entire workspace since it is difficult to link those deviations to missing physics, and (ii) those deviations can have a significant impact on other performance indexes not considered during calibration, such as stiffness, vibration or trajectory control. Thus, even if model discrepancy can be estimated in some specific cases [7], the best way to tackle this issue seems to increase the model complexity until no significant changes are found in the model parameters [3].

Acknowledgment

This work was supported by Thales Alenia Space and the Region "Provence-Alpes-Côte-d'Azur".

References

[1] C. Dumas, S. Caro, S. Garnier, and B. Furet, "Joint stiffness identification of six-revolute industrial serial robots," *Robotics and Computer-Integrated Manufacturing*, vol. 27, no. 4, pp. 881 – 888, 2011.

[2] M. Rognant, E. Courteille, and P. Maurine, "A systematic procedure for the elastodynamic modeling and identification of robot manipulators," *IEEE Trans. on Robotics*, vol. 26, no. 6, 2010.

[3] B. W. Mooring and S. S. Padavala, "The effect of kinematic model complexity on manipulator accuracy," in *Robotics and Automation*, vol. 1, May 1989.

[4] J. Wang and O. Masory, "On the accuracy of a stewart platform - part i. the effect of manufacturing tolerances," in *Robotics and Automation*, vol. 1, May 1993, pp. 114 –120.

[5] O. Masory, J. Wang, and H. Zhuang, "Kinematic modeling and calibration of a stewart platform," *Advanced Robotics*, vol. 11, no. 5, pp. 519–539, 1997.

[6] J. Chen and L. Chao, "Positioning error analysis for robot manipulators with all rotary joints," in *IEEE Int. Conf. on Robotics and Automation (ICRA)*, vol. 3, San Francisco CA USA, Apr. 1986, pp. 1011 – 1016.

[7] P. Arendt, D. W. Apley, and W. Chen, "Quantification of model uncertainty: Calibration, model discrepancy, and identifiability," *ASME Journal of Mechanical Design*, vol. 134, p. 100908, Oct. 2012.

[8] C. W. Wampler, J. M. Hollerbach, and T. Arai, "An implicit loop method for kinematic calibration and its application to closed-chain mechanisms," *IEEE Trans. on Robotics and Automation*, vol. 11, no. 5, pp. 710–724, Oct. 1995.

[9] J.-P. Merlet, "Articulated device, for use in particular in robotics," Patent 5 053 687, 1991.

[10] G. Chen, X. Liu, and Y. Du, "Elliptical-arc-fillet flexure hinges: Toward a generalized model for commonly used flexure hinges," *ASME Journal of Mechanical Design*, vol. 133, no. 8, p. 081002, 2011.

[11] T. Gayral and D. Daney, "Experimental calibration of an active space telescope with flexure joints," INRIA, Research Report RR-8096, Oct. 2012.

[12] R. M. Haralick, H. Joo, C.-N. Lee, X. Zhuang, V. G. Vaidya, and M. B. Kim, "Pose estimation from corresponding point data," *IEEE Trans. on Systems, Man and Cybernetics*, vol. 19, no. 6, pp. 1426 –1446, 1989.

[13] T. Niaritsiry, N. Fazenda, and R. Clavel, "Study of the sources of inaccuracy of a 3 DOF flexure hinge-based parallel manipulator," in *Robotics and Automation*, vol. 4, May 2004, pp. 4091 – 4096.

[14] D. Daney, Y. Papegay, and B. Madeline, "Choosing measurement poses for robot calibration with the local convergence method and tabu search," *Int. Journal of Robotics Research*, vol. 24, no. 6, pp. 501–518, 2005.

[15] A. Nahvi and J. M. Hollerbach, "The noise amplification index for optimal pose selection in robot calibration," in *IEEE Int. Conf. on Robotics and Automation (ICRA)*, vol. 1, Minneapolis, 1996, pp. 647–654.

[16] Y. Sun and J. M. Hollerbach, "Observability index selection for robot calibration," in *Robotics and Automation*, May 2008, pp. 831–836.

[17] B. Mooring, M. Driels, and Z. Roth, *Fundamentals of Manipulator Calibration*. New York, NY, USA: John Wiley & Sons, Inc., 1991.